Molecular Simulation
Vol. 00, No. 00, Month 200x, 1–24

RESEARCH ARTICLE

Semi-analytical mean-field model for predicting breathing in Metal-Organic Frameworks

L. Vanduyfhuys[a], A. Ghysels[a], S.M.J. Rogge[a], R. Demuynck[a] and V. Van Speybroeck[a]*

[a] *Center for Molecular Modeling (CMM), Ghent University, Technologiepark 903, 9052 Ghent, Belgium, (Member of the QCMM Ghent-Brussels Alliance Group)*

(*vx.x released XX 2015*)

A new semi-analytical mean-field model is proposed to rationalize breathing of MIL-53 type materials. The model is applied on two case studies, the guest-induced breathing of MIL-53(Cr) with CO_2 and CH_4, and the phase transformations for MIL-53(Al) upon xenon adsorption. Experimentally, MIL-53(Cr) breathes upon CO_2 adsorption, which was not observed for CH_4. This result could be ascribed to the stronger interaction of carbon dioxide with the host matrix. For MIL-53(Al) a phase transition from the large pore phase could be enforced to an intermediate phase with volumes of about $1160 - 1300$ Å^3, which corresponds well to the phase observed experimentally upon xenon adsorption. Our thermodynamic model correlates nicely with the adsorption pressure model proposed by Coudert et al. Furthermore the model can predict breathing behavior of other flexible materials, if the user can determine the free energy of the empty host, the interaction energy between a guest molecule and the host matrix and the pore volume accessible to the guest molecules. This will allow to generate the osmotic potential from which the equilibria can be deduced and the anticipated experimentally observed phase may be predicted.

Keywords: Thermodynamic model, osmotic ensemble, breathing, flexible frameworks, metal-organic frameworks

1 Introduction

Breathing materials are a fascinating class of flexible porous frameworks. They may undergo a substantial volume change up to 40 % under influence of external stimulus such as temperature, mechanical pressure, or gas adsorption, meanwhile maintaining their crystallographic connectivity[1–4]. An exemplary breathing metal-organic framework (MOF) is the MIL-53 family of materials, first synthesized in 2002 in the Férey group.[5] The network of metal clusters (M^{III}=Al, Cr, V, Fe, ...) and terephthalate linkers forms one-dimensional channels (see Fig. 1).

Within the family of MIL-53 materials, a number of systems have been studied with variations in the metal at the nodal points, the type of linker, ... Depending on the specific nature of the material, various stimuli were found to induce the breathing such as temperature[6–8], pressure[7, 9], guest molecules[5, 7, 10], ... Furthermore some materials were found not to breathe such as MIL-53(Fe)[11]. An overview of some of the materials and the conditions to induce breathing can be found in Refs. 3, 4. Figure 1 illustrates the various phases that are involved in the breathing processes of MIL-53(Al) and MIL-53(Cr).

*Corresponding author. Email: Veronique.VanSpeybroeck@Ugent.be

ISSN: 1351-847X print/ISSN 1466-4364 online

DOI: 10.1080/1351847YYxxxxxxxx
http://www.informaworld.com

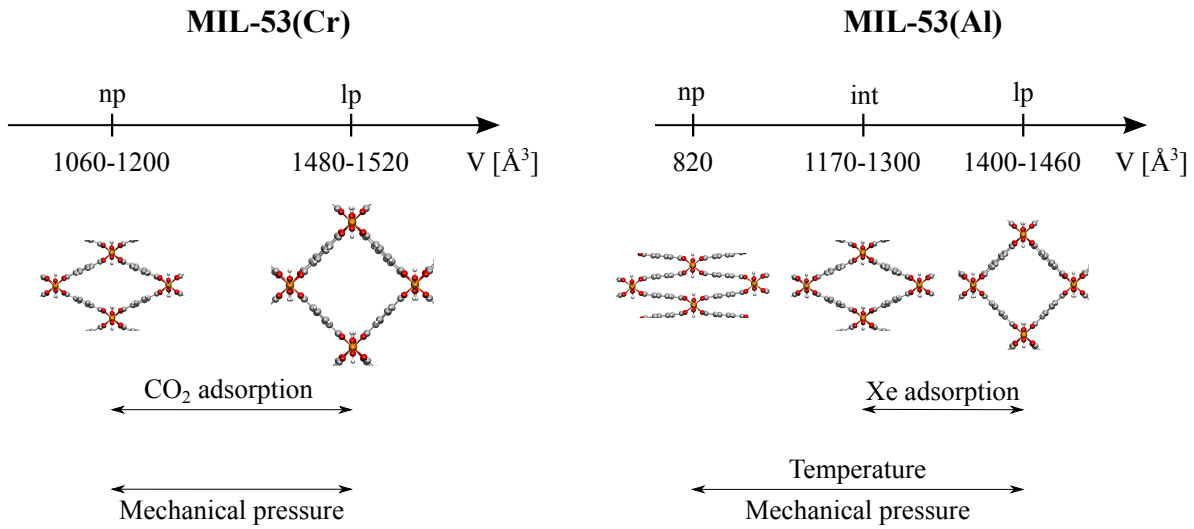

Figure 1. Illustration of the various phases involved in the breathing processes of MIL-53(Cr) and MIL-53(Al). The arrows indicate the phases and corresponding volumes that are accessible for the material during a specific breathing process (denoted above or below the arrow).

MIL-53(Cr) is found in its large-pore shape at low pressure and ambient temperature. Mechanical pressure can induce a transition to its narrow-pore (np) shape[7]. Gas adsorption can also cause an lp to np transition and, surprisingly, subsequently an np to lp transition at higher gas pressures. Not all gases induce the breathing behavior and the phenomenon is usually only observed in a specific temperature range. For instance, CO_2 makes MIL-53(Cr) breathe with hysteresis between the adsorption and desorption isotherm, while CH_4 does not cause a transition at 300 K.

MIL-53(Al) is a material for which a transition between the large and narrow pore was observed experimentally for the empty material and under the influence of temperature as sole stimuli[6]. As a result this material received also considerable interest from theory. Various studies appeared on the intrinsic bistable behavior of the framework and the occurrence of two minima on the potential energy surface. Walker et al. indeed found two minima on the potential energy surface provided that dispersion interactions were taken into account in the first principle energy calculations[12]. Fig. 1 schematically shows the large pore (lp) and narrow pore (np) of the empty host. In 2012, some of the present authors derived a first principle flexible force field for MIL-53(Al), which was able to reproduce an energy profile exhibiting two minima in terms of the breathing angle[13]. Furthermore, the force field was used to succesfully reproduce the pressure-induced breathing of the empty framework[9]. Several other force fields also exist that present two distinct minima for the chromium variant of MIL-53.[7, 14] These theoretical calculations gave seminal insight into the nanoscale interactions enforcing breathing. One must however be careful when rationalizing breathing solely on basis of potential energy curves at 0 K. The occurrence of certain macroscopically observed phases is a result of a thermodynamic process and thus one should describe the phenomenon in the correct thermodynamic ensemble. Boutin et al. studied the breathing behavior of MIL-53(Al) upon Xenon adsorption and found breathing transitions in the measured adsorption isotherms in the temperature range $195 - 323$ K[15]. They also developed a thermodynamic model to explain the observed behavior of the material. Under influence of Xe-adsorption, the materials shrinks to a phase with a volume in between those of the empty narrow pore and large pore. To be consistent with Bousquet et al.[16]we denote this as an intermediate phase (int on Fig. 1).

A multitude of theoretical papers appeared using various thermodynamic models to rationalize the breathing. It is impossible to give a complete overview here, but for the readability of the

current paper, some landmark papers are highlighted hereafter. Coudert et al. described the structural transitions in MIL-53(Al) by comparing the grand potential in the osmotic ensemble in the large and narrow pore based on experimental data[17]. They later used the same model to derive a generic temperature-loading phase diagram[18]. Neimark et al. developed a stress-based model by defining an osmotic stress which initiated the transition[19]. Triguero et al. proposed a deformation mechanism of the transition that occured by a layer-by-layer shear and thus subsequent two-dimensional layers were not in the same form[20]. Previous molecular explanations of the phase transition were based on the free energy comparison of two distinct phases. In 2012 Bousquet et al. introduced a Wang-Landau based Monte Carlo sampling method which allowed an efficient sampling of the osmotic ensemble, which thus also allowed to study the free energy landscapes as function of the volume[21]. Recently some of the presenting authors introduced a generic free energy model for MIL-53(Cr) and adsorbed gases[22], which included three contributions: the host free energy, the guest-guest interactions and the host-guest interactions. As a result the free energy landscape could be constructed scanning all shapes and a variable amount of adsorbed guest molecules. We were able to determine which shapes are the most stable in terms of control variables such as the adsorbing gas chemical potential and the external pressure. The phase behavior of MIL-53 for a given (μ, P) could be predicted by minimizing the osmotic potential $\tilde{X}$ with respect to volume and number of adsorbed guest particles. Increasing the chemical potential of CO_2 was seen to destabilize the lp shape, since the increasing amount of adsorbed CO_2 gradually favored the interaction in the np shape, resulting in the lp$\rightarrow$np transition. In accordance with experiment the lp$\rightarrow$np transition followed at increasing the chemical potential of CO_2, when the lp shape is favored because of its more spacious pore volume accomodating more particles.

In this paper we present a new semi-analytical mean-field model to predict and understand the breathing phenomenon in flexible materials. The model is based on the free energy of the empty host profile, the free energy among guest particles and the interaction free energy between the guest and the host material. A semi-analytical procedure is presented to minimize the osmotic potential, in which all contributions have an analytical functional form and the minimization is done numerically. The osmotic ensemble with a constant number of MOF unit cells (n), varying number of guest molecules (N) controlled by the external chemical potential (μ), varying cell volume (V) controlled by the external mechanical pressure (P) and temperature (T), is the thermodynamic ensemble that resembles a standard adsorption experiment the closest. The phase behavior of a flexible material can be predicted by minimizing the osmotic potential $\tilde{X}$ as function of the volume V and the number of adsorbed guest particles N. The minimizations towards volume and number of adsorbed particles are not performed simultaneously but in two subsequent steps, allowing to compute intermediate volume-dependent contributions to the osmotic potential and unravel the physical processes that lie at the basis of breathing. The semi-analytical model is tested on two well known case studies : the MIL-53(Cr) for which a phase transition was observed upon adsorption of CO_2 at room temperature while this was not the case for CH_4 and MIL-53(Al) for which recently new data appeared on the breathing behavior upon Xenon adsorption[15].

In our earlier thermodynamic model, the osmotic potential $\tilde{X}$ was minimized with respect to the volume and the number of guest molecules numerically. The free energy expression was written in an analytical form. The minimization boils down to imposing two minimization conditions, namely the derivatives with respect to volume and number of particles needs to be zero. This results in an equilibrium condition for the chemical potential and for the pressure. In this work the equilibrium condition for the chemical potential is solved as far as possible analytically, which allows to interpret important thermodynamic variables in a physically founded way. A key quantity that will be introduced is the fill factor which describes the density of guest molecules in the pores. Almost all thermodynamic quantities will be interpreted in

terms of this fill factor.

The semi-analytical model is tested on the well studied MIL-53(Cr) system and for this material the here presented study is an extension of our earlier theoretical model. Our second case study concerns MIL-53(Al) adsorbed with Xenon guest particles. For this system, all input quantities are derived from first principles, thus no empirical input was used. The free energy profile of the empty host was determined on the basis of molecular dynamics (MD) simulations in an ensemble that keeps the volume fixed but for which simultaneously volume-conserving deformations of the unit cell are allowed. The molecular dynamics simulations are performed using our own first principle flexible derived force field[13]. This test case illustrates how guest adsorption may create an additional equilibrium volume under specific conditions that lies intermediate between the lp and np shape.

The study as presented here gives a complementary insight into the breathing behavior of flexible materials. In principle it is applicable to other materials and should allow to predict under which conditions a material would breathe. The remainder of this paper is organized as follows. In Section 2 all contributions to the free energy are introduced as well as how to calculate them. The Legendre transform to the osmotic ensemble, the resulting equilibrium conditions and how to solve them are also explained in Section 2. The computational details are outlined in Section 3. In Section 4, the presented model is applied to methane and carbon dioxide adsorption in MIL-53(Cr) and to xenon adsorption in MIL-53(Al). Finally, the main conclusions are formulated in Section 5.

2 Methodology

The methodology section consists of two parts, first the expression of the Helmholtz free energy is introduced and second a Legendre transform is conducted to transform the free energy towards the thermodynamic potential $\tilde{X}$ in the osmotic ensemble. This last step is necessary to connect the theoretical model with the experimental conditions for describing the adsorption-induced breathing. The innovative aspect of our semi-analytical model must be sought in the method to minimize the osmotic potential in a semi-analytical way.

2.1 *Free energy model*

The starting point for the thermodynamic analysis is the Helmholtz free energy F of the system as a function of the following macroscopic parameters: number of host unit cells n, number of adsorbed guest molecules N, host unit cell volume V and temperature T. This means that our system is originally described in the (n, N, V, T) ensemble, which is ideally suited to deduce molecular level properties. Afterwards a transformation will be conducted towards the osmotic ensemble, i.e. the (n, μ, P, T) ensemble (see 2.2).

The free energy of the entire system, i.e. host framework with adsorbed guest molecules, can be written as:

$$F\left(n, N, V, T\right) = F_{\text{host}}\left(n, V, T\right) + F_{\text{guest}}\left(n, N, V, T\right) + F_{\text{int}}\left(n, N, V, T\right) \tag{1}$$

F_{host} is the free energy of the empty host, i.e. in absence of guest molecules. F_{guest} is the free energy of the guest molecules, which interact among each other but are confined in the pore volume of the host framework without interacting with the framework. Finally, F_{int} consists of the remaining contribution, which is the interaction of the guest molecules with the host framework.

In this paper, the thermodynamic limit is used, assuming a large sample of framework unit cells: $n \to +\infty$ and $N \to +\infty$ with $\frac{N}{n} = cte$. In this limit, the total free energy becomes linear in the number of host unit cells (see Section 2 in the Supporting Information). Hence, the framework can be restricted to a single unit cell $n = 1$ if all extensive observables are interpreted as being defined per unit cell. For example, the free energy F and number of adsorbed molecules N represent the free energy and number of adsorbed molecules per unit cell respectively. From now on, n is set to 1 and is dropped from the equations. Furthermore, the system is studied at a fixed temperature of 300 K. Hence, temperature will be a fixed parameter in all equations. Eq. (1) now becomes:

$$F\left(N,V\right) = F_{\text{host}}\left(V\right) + F_{\text{guest}}\left(N,V\right) + F_{\text{int}}\left(N,V\right) \tag{2}$$

The remaining part of this subsection is devoted to discussing all three contributions and how to compute them from molecular simulations.

2.1.1 Host free energy: F_{host}

The first contribution F_{host} to the free energy in our thermodynamic model is that of the empty host framework as a function of the unit cell volume V. For the MIL-53(Cr) system, the same F_{host} is taken as in Ref. 22 for the sake of comparison.

For MIL-53(Al) the free energy profile $F_{\text{host}}(V)$ is determined using thermodynamic integration and molecular dynamics simulations. Molecular dynamics simulations are performed at a series of fixed volumes, while allowing unit cell shape fluctuations. Indeed, metal-organic frameworks often do not have a cubic unit cell, which implies that both volume and shape are independent degrees of freedom. The idea is based on rewriting the cell tensor $\bar{\bar{h}}$ as the product of the volume $V = \det(\bar{\bar{h}})$ and the cell shape tensor $\bar{\bar{h}}_0$:

$$\bar{\bar{h}} = V^{1/3}\bar{\bar{h}}_0 \tag{3}$$

where $\det(\bar{\bar{h}}_0) = 1$. Analogously, the total stress tensor $\bar{\bar{\sigma}}$ is rewritten as the product of the hydrostatic pressure $P = \text{Tr}(\bar{\bar{\sigma}})/3$ and a stress anisotropy tensor $\bar{\bar{\sigma}}_0$ with $\text{Tr}(\bar{\bar{\sigma}}_0) = 1$, so that

$$\bar{\bar{\sigma}} = 3P\bar{\bar{\sigma}}_0 \tag{4}$$

Hence, to constrain the volume V without constraining the cell shape $\bar{\bar{h}}_0$, our MD simulation is carried out in the (n,V,$\bar{\bar{\sigma}}_0$,T) ensemble. This ensemble can easily be implemented starting from the hybrid method formulation of the isothermal-isobaric ensemble as introduced by Martyna et al.[23] by explicitly setting $\dot{V} = 0$.

During the MD simulations, the derivative $-\dfrac{\partial F_{\text{host}}}{\partial V}$ is measured, and its average, which is the pressure $P_{\text{host}}(V)$, is integrated numerically to find the profile $F_{\text{host}}(V)$:

$$F_{\text{host}}(V) - F_{\text{host}}(V_{\text{ref}}) = \int_{V_{\text{ref}}}^{V} \left(\frac{\partial F_{\text{host}}}{\partial V'}\right) dV' = -\int_{V_{\text{ref}}}^{V} P_{\text{host}}(V')dV' \tag{5}$$

The reference volume V_{ref} and its free energy $F_{\text{host}}(V_{\text{ref}})$ may be chosen arbitrarily, and are here set such that the free energy of the absolute minimum is zero. To mimic the experimental conditions, it is assumed that the system is under isotropic stress, i.e. $\bar{\bar{\sigma}}_0 = \bar{\bar{1}}/3$.

One point that needs special attention is the procedure to generate the initial structures corresponding to the volume grid mentioned earlier. Herefore, an MD simulation in the conven-

tional (n, P, T) ensemble is carried out with a certain isotropic pressure P, starting from the large pore structure, where the cell volume is allowed to fluctuate. When the applied pressure P is sufficiently high, this large pore structure will collapse into the narrow pore structure, hence sweeping through all available volumes between V_{lp} and V_{np}. The initial structure corresponding to a specific volume V_0 in the volume grid, is taken as a snapshot from this (n, P, T) simulation at the moment where the simulated volume V is within 0.5 $\mathrm{\AA}^3$ of V_0. The remaining mismatch between V and V_0 is removed by rescaling the simulated cell tensor and positions by $(V_0/V)^{1/3}$.

The molecular dynamics simulations for MIL-53(Al) are performed using our in-house developed flexible force field[13]. The energy expression has a covalent, an electrostatic and a van der Waals contribution. The covalent terms consist of harmonic bonds, harmonic bends and single-cosine dihedral terms, which were all fitted to reproduce the *ab initio* Hessian and geometry of two well-chosen clusters corresponding to the organic linker and inorganic metal-oxide respectively. The electrostatic part is described by means of Coulomb interactions between point charges, which were derived from an Hirshfeld-I scheme applied on the valence molecular electron density. The van der Waals terms were taken from the MM3 force field of Allinger et al.[24]; however, they were rescaled with a factor of 0.86 in order to reproduce the experimental value of the large pore to narrow pore transition pressure of the empty host[9]. Recently we proposed an automated protocol to derive flexible force fields from first principles for metal organic frameworks[25]. The procedure is called QuickFF as it allows to generate a reliable force field with a minimal number of manual interventions. QuickFF can be used to generate force fields for MOFs that can be used to compute the required free energy profiles of the emtpy host. Several other force field protocols have been developed by other groups, such as MOF-FF[26], BTW-FF[27] and UFF4MOF[28].

2.1.2 Guest free energy: F_{guest}

The second contribution to the free energy is that of the guest molecules confined within pores of the framework without taking into account the interaction with the host. This contribution can be modeled as a van der Waals gas confined in a volume V_{p}. The expression for the guest free energy has the well-known form of a van der Waals gas:

$$F_{\mathrm{guest}}(N, V) = k_B T \ln N! - N k_B T \ln \left[\frac{P_0}{k_B T} \left(V_p(V) - bN \right) \right] - \frac{aN^2}{V_p(V)} + N\mu_0 \tag{6}$$

where $V_p(V)$ is the pore volume as function of the unit cell volume, a and b are the van der Waals parameters and $\mu_0 = k_B T \ln \frac{P_0 \Lambda^3}{k_B T}$ is a reference chemical potential, representing the chemical potential of an ideal gas at temperature T and pressure P_0 (P_0 is arbitrarily chosen). The pore volume $V_p(V)$ can be derived from Monte Carlo simulations with Widom insertions for a range of volumes. To simplify the simulation protocol, we use a rigid framework at each volume with a shape defined as the zero-kelvin equilibrium at that particular volume and the structures are the same as used in Ref. 13 to calculate the energy profile at 0 K.

2.1.3 Interaction free energy: F_{int}

The interaction free energy is the difference between the exact total free energy F and the sum of the empty host free energy and guest free energy $F_{\mathrm{host}} + F_{\mathrm{guest}}$ (see Eq. 1). Following the approach of Ref. 22, the interaction term is computed with a mean field approximation. This mean field approximation implies three assumptions: the intermolecular interaction energy can be calculated with a rigid host framework, the interaction free energy of N guest molecules is equal to N times the interaction free energy of one particle and the interaction entropy of one particle is negligible. Using these approximations, the interaction free energy becomes (explicit

proof given in Section 1 of the Supporting Information):

$$F_{\text{int}}(N,V) = N \cdot \Delta U(V) \tag{7}$$

$$\Delta U(V) = \frac{\int U_{\text{int}}(\langle \boldsymbol{R} \rangle_{NVT}, \boldsymbol{r}) e^{-\beta U_{\text{int}}(\langle \boldsymbol{R} \rangle_{NVT}, \boldsymbol{r})} d\boldsymbol{r}}{\int e^{-\beta U_{\text{int}}(\langle \boldsymbol{R} \rangle_{NVT}, \boldsymbol{r})} d\boldsymbol{r}} \tag{8}$$

$\langle \boldsymbol{R} \rangle_{NVT}$ is the vector containing the (fixed) coordinates of all host atoms corresponding to the equilibrium at a temperature T and unit cell volume V. and $\boldsymbol{r}$ is the vector containing the coordinates of a single guest molecule.

2.2 *Legendre transform and osmotic potential*

The starting point of our thermodynamic model is the free energy $F(n,N,V,T)$ in Eq. (1) as a function of number of host unit cells n, number of adsorbed particles N, unit cell volume V and temperature T. In an experimental setup to investigate the breathing behavior of a metal-organic framework, however, one typically controls the mechanical pressure on the MOF, the chemical potential of the adsorbent species in the environment and the temperature. Usually, the mechanical pressure is exerted by the adsorbent species surrounding the MOF. This means that the imposed pressure and chemical potential are coupled by means of the equation of state $P = P(\mu)$ of the adsorbent molecules in the evironment. Hence, the free energy F in the (n,N,V,T) ensemble needs to be transformed to the thermodynamic potential X in the osmotic ensemble (n,μ,P,T). This transformation is done by means of the Legendre transform:

$$X(\mu,P) = \min_{(N,V)} \{F(N,V) + PV - \mu N\} \tag{9}$$

In Ref. 22, the minimization is performed by computing $F + PV - \mu N$ on a (N,V) grid and finding the minimum. In this work, the minimization is performed in a semi-analytical way as explained hereafter. First, define an intermediate potential $\tilde{X}_{\mu P}(N,V) = F + PV - \mu N$ in which N and V are treated as independent variables and μ and P as fixed parameters. Next, the thermodynamic potential X for a certain value of μ and P is defined as the minimum of the potential $\tilde{X}_{\mu P}$:

$$\frac{\partial \tilde{X}_{\mu P}}{\partial N} = 0 \quad \rightarrow \quad \frac{\partial F_{\text{guest}}}{\partial N} + \frac{\partial F_{\text{int}}}{\partial N} = \mu \tag{10}$$

$$\frac{\partial \tilde{X}_{\mu P}}{\partial V} = 0 \quad \rightarrow \quad -\frac{\partial F_{\text{host}}}{\partial V} - \frac{\partial F_{\text{guest}}}{\partial V} - \frac{\partial F_{\text{int}}}{\partial V} = P \tag{11}$$

A solution is stable when the matrix of second order derivatives is positive definite. Eqs. (10-11) represent a balance in chemical potential and pressure terms. When substituting the various contributions of the free energy F as introduced in the previous section, the chemical and mechanical equilibrium expressions read, respectively:

$$\mu_{\text{guest}}(N,V) + \mu_{\text{int}}(V) = \mu \tag{12}$$

$$\mu_{\text{guest}}(N,V) = k_B T \ln\left(\frac{bN}{V_p(V) - bN}\right) + \frac{bNk_BT}{V_p(V) - bN} \tag{13}$$

$$- \frac{2aN}{V_p(V)} + \mu_0 - k_B T \ln\left(\frac{P_0 b}{k_B T}\right) \tag{14}$$

$$\mu_{\text{int}}(V) = \frac{\partial F_{\text{int}}}{\partial N} = \Delta U(V) \tag{15}$$

and

$$P_{\text{host}}(V) + P_{\text{guest}}(N,V) + P_{\text{int}}(N,V) = P \tag{16}$$

$$P_{\text{host}}(V) = -\frac{\partial F_{\text{host}}}{\partial V} \tag{17}$$

$$P_{\text{guest}}(N,V) = \left[\frac{Nk_BT}{V_p(V) - bN} - a\left(\frac{N}{V_p(V)}\right)^2\right]\frac{\partial V_p}{\partial V} \tag{18}$$

$$P_{\text{int}}(N,V) = -N\frac{\partial \Delta U}{\partial V} \tag{19}$$

Solving these equations simultaneously for given (μ, P) results in the solution of $(N_{\mu P}, V_{\mu P})$ for every (μ, P). This solution can then be substituted in $\tilde{X}_{\mu P}$, which results in the thermodynamic potential $X(\mu, P)$. In this work, however, Eqs. (12) and (16) are solved in two subsequent steps. The solution remains exact, however, it will allow the construction and interpretation of intermediate results that can be usefull to understand the breathing mechanism. First, the chemical potential equation (Eq. 12) is solved for the number of particles N, which results in the number of particles as a function of the unit cell volume for every value of the chemical potential $N_\mu(V)$. Next, this solution $N_\mu(V)$ is substituted in Eq. (16) and solved for the volume, resulting in the equilibrium volume $V_{\mu P}$. The number of particles $N_{\mu P}$ is then readily available as $N_\mu(V_{\mu P})$. As mentioned earlier, the solution of Eqs. (10) and (11) needs to be stable, i.e. correspond to a minimum. Hence, the matrix of second-order derivatives is postive definite. When solving the equations subsequently, this stability criterion is equivalent to expressing stability individually for both steps (see also Section 4 of the Supporting Information):

$$\frac{\partial^2 \tilde{X}_{\mu P}}{\partial N^2} > 0 \tag{20}$$

$$\frac{d^2}{dV^2}\left[\tilde{X}_{\mu P}\left(N_\mu(V), V\right)\right] > 0 \tag{21}$$

The two subsequent steps will now be elaborated in the following subsections. The resulting general procedure to perform this Legendre transformation is illustrated in Fig. 2. The figure illustrates the required input and resulting output of both the chemical potential equilibrium (indicated in yellow on the figure) and the mechanical pressure equilibrium (indicated in blue on the figure). Specific parts of the figure will be explained in the ongoing sections.

2.2.1 The chemical potential equation

Let us first focus on the chemical potential equation (Eq. 12). A new key quantity is introduced, the fill factor f:

$$f = \frac{bN}{V_p} \tag{22}$$

As the name suggests, the fill factor represents the degree to which the pores are filled. Suppose that $f = 1$, then $N = \frac{V_p}{b}$, which is the maximum number of particles that fits in the pores assuming perfect filling, i.e. no empty space between particles. Thus b is the volume taken by one particle, which also figures in the van der Waals equation of state. Since perfect filling is impossible, the fill factor will always be smaller than one ($0 \leq f < 1$).

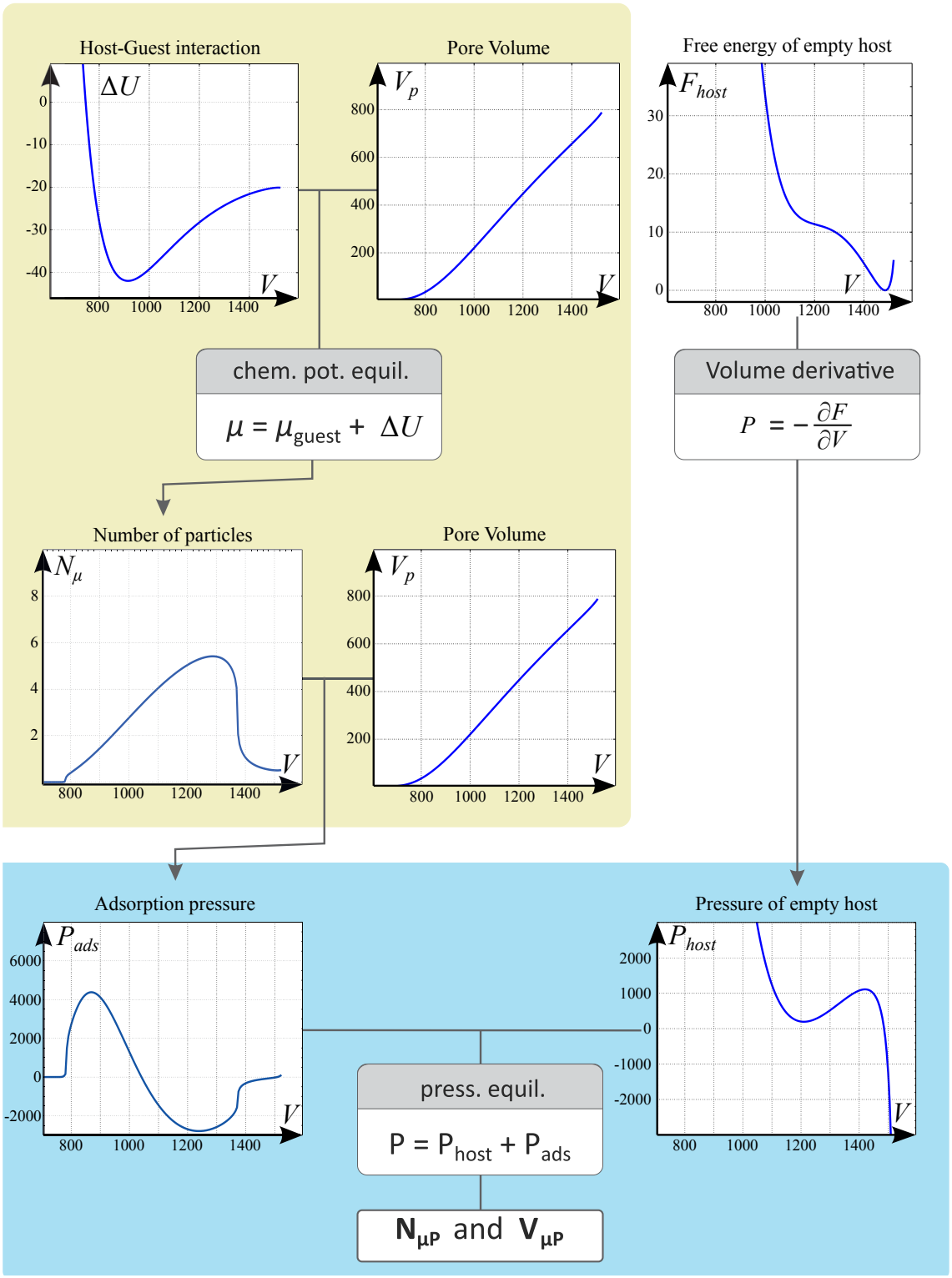

Figure 2. Illustration of the general procedure to perform the Legendre transform from the canonical ensemble to the osmotic ensemble in two subsequent steps. The yellow part represents the first step of the Legendre transformation, i.e. the chemical potential equilibrium (section 2.2.1). The blue part represents the second step of the Legendre transformation, i.e. the pressure equilibrium (section 2.2.2).

A new reference μ_0' for the chemical potential is introduced:

$$\mu_0' = \mu_0 \quad k_B T \ln\left(\frac{P_0 b}{k_B T}\right) = k_B T \ln\left(\frac{\Lambda^3}{b}\right) \tag{23}$$

it represents the chemical potential of an ideal gas at a gas density of one particle per volume b and a pressure of $\frac{k_BT}{b}$. This new reference is introduced as it allows to separate the terms independent of f and V into one term. Substituting these quantities in the chemical potential equation Eq. (12) gives:

$$\mu = k_BT \ln \frac{f}{1-f} + k_BT \frac{f}{1-f} - k_BT \cdot cf + \mu_0' + \Delta U(V) \tag{24}$$

where the short notation $c = \frac{2a}{k_BTb}$ is used for the dimensionless ratio of the van der Waals parameters. The value for c will be determined by the precise nature of the guest molecules. Thus the derivation presented so far gives a boundary condition for the fill factor f in terms of the volume V for a given chemical potential μ. After some rearrangements, the previous equation gives the following expression:

$$\frac{(\mu - \mu_0' - \Delta U(V))}{k_BT} = A(f) \tag{25}$$

where $A(f)$ is a dimensionless function of the fill factor f:

$$A(f) = \ln \frac{f}{1-f} + \frac{f}{1-f} - cf \tag{26}$$

$\mu - \mu_0'$ is the chemical potential of a guest molecule outside the MOF (relative to the reference μ_0'), ΔU is the interaction of a single guest molecule with the host framework and can also be interpreted as the increase in chemical potential inside the pores due to the interaction, and $k_BTA(f)$ represents the chemical potential of a van der Waals guest molecule inside the pores (relative to the reference μ_0'). Eq. (25) also represents the balance in chemical potential: if the interaction ΔU decreases (more favorable interaction inside the pores), then in order to balance with the chemical potential outside the MOF ($\mu - \mu_0'$), the chemical potential of the van der Waals particles inside the pores $k_BTA(f)$ will increase (more populated pores). For a given chemical potential (μ) and an interaction profile ($\Delta U(V)$), the left-hand-side of Eq. (25) is a known profile in terms of the volume. As such one can determine the fill factor for each volume by solving Eq. (25). This means that the volume dependence of the fill factor is determined by the interaction profile ΔU. The graphical representation of the solution is shown in Fig. 3 for a couple of c-values.

Solving Eq. (25) gives the fill factor $f_\mu(V)$ as a function of volume V, and as a result the number of particles that adsorb in the pores is found as a function of volume:

$$N_\mu(V) = f_\mu(V) \frac{V_p(V)}{b} \tag{27}$$

This first step of the Legendre transformation is indicated in yellow on Fig. 2. Figure 3 shows the functional dependence of $A(f)$ on the fill factor f. Three distinct situations are plotted: a low value $c = 3$, a critical value $c = 6.75$ and a high value $c = 11$. To allow a better interpretation of these numbers, some typical values of c (at 300 K) are: $c = 4.3$ for methane, $c = 6.89$ for carbon dioxide and $c = 6.41$ for xenon. An important characteristic of the function $A(f)$ needs to be discussed, which is connected to the behavior of a van der Waals gas. A van der Waals gas has a critical point, represented by a critical density of $\rho = \frac{1}{3b}$ (corresponding to a fill factor of $f = \frac{1}{3}$) and a critical temperature T_c. For a temperature above T_c, the van der Waals particles always behave as a gas. For a temperature below T_c, a phase splitting occurs according to Maxwell's rule: part of the fluid is in liquid form (with a density above $\frac{1}{3b}$), while the other part is in gas form (with a density below $\frac{1}{3b}$). Due to the connection between $A(f)$ and the chemical potential of the van der Waals gas inside the pores, one could argue

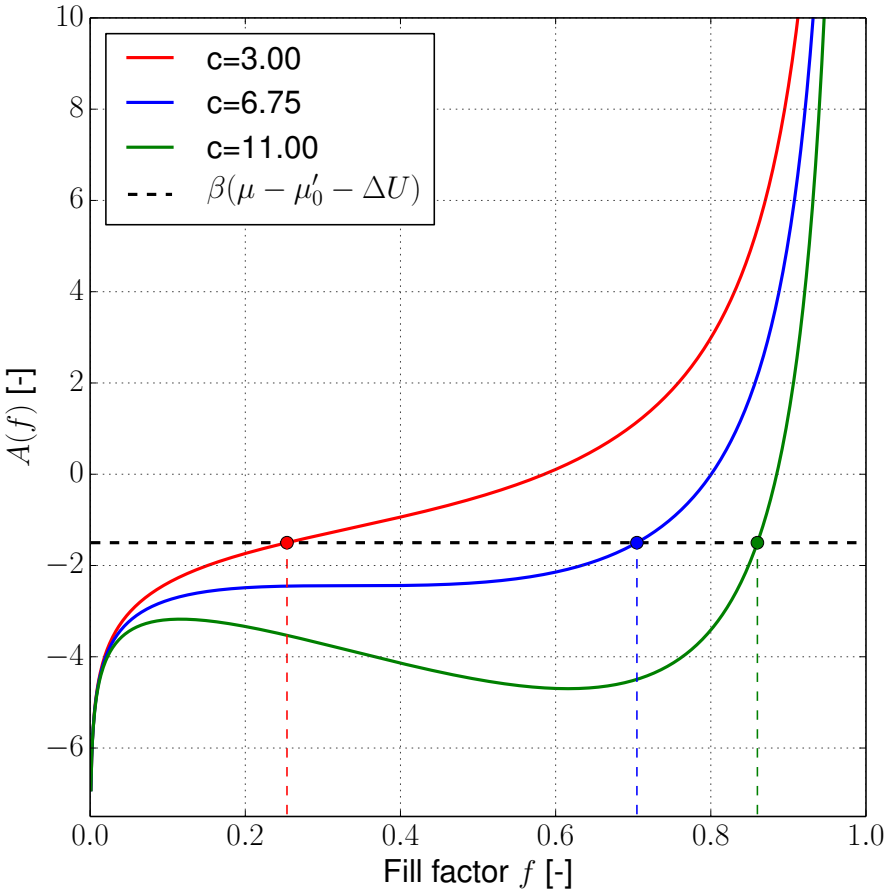

Figure 3. Graphical representation of the solution of Eq. (25).

that this behavior can be transfered to $A(f)$. When c has a value below the critical value of $c_c = 6.75$, Eq. (25) will have a single solution. However, if $c > 6.75$ the van der Waals particles inside the pores will be subject to a phase splitting. Part of the particles will be in a phase with a fill factor of $f > \frac{1}{3}$ and the other part will be in a phase with a fill factor of $f < \frac{1}{3}$. However, Maxwell's rule is not validated for van der Waals particles confined in such small volumes as in the pores of a MOF. Therefore, the occurence of phase splitting is not warranted. Instead, the particles could still be in a single phase depending on their history. In this work, however, we will only study systems with a temperature above the critical temperature. The mathematical description of this behavior is included in Section 3 of the Supporting Information. To satisfy this condition, we slightly decreased the van der Waals parameter a of carbon dioxide from 611.9 kJ mol ^{1} Å ^{3} to 599.5 kJ mol ^{1} Å ^{3} so that its critical temperature decreases from 306.1 K to 299.9 K, which is just below 300 K. For the reader's convenience we mention the that the critical temperature of methane is 192.5 K and that of xenon is 285.0 K.

2.2.2 The pressure equation

The solution $N_\mu(V)$ can now be substituted in the pressure equilibrium condition (Eq. 16):

$$P = P_{\text{host}}(V) + P_{\text{guest},\mu}(V) + P_{\text{int},\mu}(V) \tag{28}$$

$$P_{\text{host}}(V) = -\frac{\partial F_{\text{host}}}{\partial V} \tag{29}$$

$$P_{\text{guest},\mu}(V) = \frac{k_B T}{b}\left[\frac{f_\mu(V)}{1-f_\mu(V)} - \frac{c}{2}f_\mu^2(V)\right]\frac{\partial V_p}{\partial V} \tag{30}$$

$$P_{\text{int},\mu}(V) = -f_\mu(V)\frac{V_p(V)}{b}\frac{\partial \Delta U}{\partial V} \tag{31}$$

Eq. (28) is solved graphically for the volume by finding the intersect of the total pressure $P_{\text{host}}(V) + P_{\text{guest},\mu}(V) + P_{\text{int},\mu}(V)$ with a horizontal line at pressure P, i.e. the external control pressure. This results in the equilibrium volume $V_{\mu P}$ for a certain value of the chemical potential and pressure. Substituting this equilibrium volume in Eq. (27) gives us the equilibrium number of particles:

$$N_{\mu P} = N_\mu(V_{\mu P}) = f_\mu(V_{\mu P})\frac{V_p(V_{\mu P})}{b} \tag{32}$$

The stability condition (Eq. 21) can graphically be interpreted in two ways: the thermodynamic potential $\tilde{X}_{\mu P}\left(N_\mu(V), V\right)$ should have a minimum at $V_{\mu P}$ or the total pressure $P_{\text{host}}(V) + P_{\text{guest},\mu}(V) + P_{\text{int},\mu}(V)$ should have a negative slope at $V_{\mu P}$. This second step of the Legendre transformation is indicated in blue on Fig. 2.

3 Computational details

In this paper two case studies will be considered: the MIL-53(Cr) upon adsorption with CO_2 and CH_4 and the MIL-53(Al) upon adsorption with xenon.

3.1 *Input parameters for MIL-53(Cr) with CO_2 and CH_4:*

For MIL-53(Cr) all input parameters were taken similar as in our previous study for the sake of comparison[22]. The free energy profile of the empty host was postulated in that paper on basis of a careful comparison with experimental data. The pore volume and interaction energy were calculated in the same way as in this work. More information about the computational details of those calculations can be found in Ref. 22. For the transparency of the current paper the host profile is shown in Fig. 4.

3.2 *Input parameters for MIL-53(Al) with Xe:*

All required input was obtained from molecular simulations with our in-house developed simulation code YAFF[29] using our own force field[13]. The free energy profile of the empty host at the required temperatures is generated using the procedure described in section 2.1.1, which relies on MD simulations in the $(n, V, \bar{\bar{\sigma}}_0, T)$ ensemble. To this end MD simulations are carried out of 800 ps with a Verlet integration time step of 0.5 fs using our own flexible force field with a rescaling factor of 0.86 for the van der Waals interactions. This factor was determined to obtain a quantitative agreement for the transition pressure observed in compression–decompression cycles for MIL-53(Al)[9]. A simulation cell containing 152 atoms (two conventional unit cells) is created by doubling the unit cell along the axis of the metal

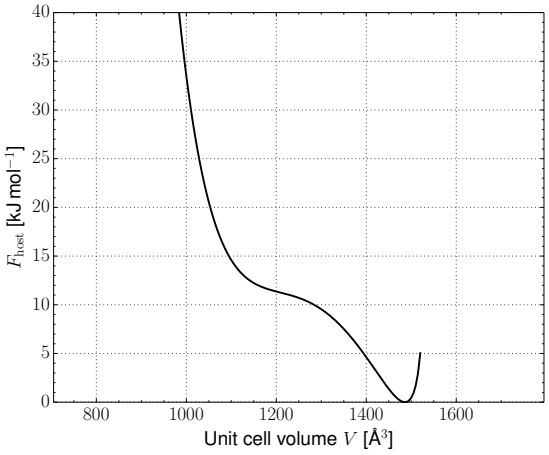

Figure 4. The host free energy as function of unit cell volume for MIL-53(Cr) from Ref. 22.

oxides. Electrostatic contributions are efficiently calculated using the Ewald summation and a real-space cutoff radius of 15 Å. The correct temperature distribution at 300 K is ensured via a Nosé–Hoover thermostat chain with three beads and a coupling time constant of 0.1 ps. This combination of parameters is shown to yield the desired distribution, and does not suffer from a lack of ergodicity.[30]

The desired pressure distribution is achieved by applying the barostat suggested by Martyna, Tobias, Tuckerman and Klein with a coupling constant of 1 ps.[23] For the simulation in the (n, P, T) ensemble, a hydrostatic pressure of 1 MPa is imposed, while for the simulations in the $(n, V, \bar{\bar{\sigma}}_0, T)$ ensemble, only the requirement of a hydrostatic pressure is imposed.

To obtain the pore volume and the interaction energy of a single xenon atom with the MIL-53(Al) host, Monte Carlo simulations with Widom insertions are performed. A guest atom is inserted at 10^5 uniformly distributed positions in the unit cell of rigid host structures. The Buckingham terms in the van der Waals part of the force field were converted to Lennard-Jones terms to avoid the unphysical region of the Buckingham potential at small interatomic distances. The conversion was implemented by imposing that the depth and position of the minimum for the Lennard-Jones potential should be identical to that of the Buckingham potential. The interaction energy U_{int} can be obtained from the simulation by applying Eq. (8), while the pore volume V_p is obtained from the Widom insertion method using a helium probe. The Rosenbluth factor is adjusted with a Heaviside function to avoid that negative interaction energies result in prefered regions of space (due to a Boltzmann factor larger than 1):

$$V_p = \frac{V}{N_{MC}} \sum_{i=1}^{N_{MC}} e^{\ \beta U_{\text{int}}(\boldsymbol{r}_i) H[U_{\text{int}}(\boldsymbol{r}_i)]} \tag{33}$$

with N_{MC} the number of insertions. All the required input data, i.e. the empty host free energy, the pore volume and the interaction energy, are calculated on a discrete grid of the unit cell volume. However, for the thermodynamical analysis, we require all the free energy contributions as analytical functions of unit cell volume. Therefore, the discrete grid data are fit to high-order Taylor expansions in terms of the unit cell volume. More details can be found in Section 4 of the Supporting Information.

4 Results and Discussion

4.1 *Case study I: methane and carbon dioxide in MIL-53(Cr)*

In this section the model is applied to MIL-53(Cr) with methane and carbon dioxide. In principle, the chemical potential and mechanical pressure are independent thermodynamic variables. However, in an adsorption/desorption experimental setup, the guest molecules in the environment of the MOF exert a mechanical pressure on the MOF, and this is the only source of pressure. This means that the chemical potential μ and mechanical pressure P are coupled through the equation of state $P = P(\mu)$ of the gas.

4.1.1 Number of adsorbed particles from the chemical potential equation

As outlined in the Methodology section, the first step is to solve Eq. (25) for the fill factor f. As a result the number of particles can be computed as a function of the volume. In Fig. 5 the f_μ and N_μ curves are plotted for several values of the chemical potential μ. In this work, whenever an observable is denoted with a symbol containing μ and/or P in the subscript, it indicates the solution of the chemical potential and/or mechanical pressure equation. For clarity of the interpretation, the chemical potential must be interpreted as the potential felt by the particles outside of the material. Since particles favor regions of low chemical potential, this means that more negative values of the chemical potential result in particles that prefer to reside outside of the host material. The figure clearly shows a peak that starts to grow at low volumes for both gases, which demonstrates that both gases initially adsorb more in the narrow pore than in the large pore. However, closer inspection of the chemical potential for both gases, clearly reveals that carbon dioxide starts to fill up the pores at much lower chemical potentials than methane (filling starts at $-74\ \mathrm{kJ\,mol^{-1}}$ for carbon dioxide versus $-57\ \mathrm{kJ\,mol^{-1}}$ for methane). These results confirm earlier observations that both gases prefer to adsorb in the narrow pore and carbon dioxide interacts more strongly with the framework than methane. At this point it is interesting to correlate these results to the earlier equations that we derived. Indeed, it was found that the function $A(f)$ depends on the difference between the chemical potential (relative to a reference value μ_0') and the interaction potential. Thus the stronger the particle interacts with the material, the larger the driving force for being adsorbed in the material. Finally, the results show that the pores can be filled up to a maximum fill factor of around $f = 0.9 - 0.95$, suggesting that there is around $5 - 10$ % of empty space between the molecules.

4.1.2 Adsorption isotherm from the pressure equation

After solving the chemical potential equation, the solution for the number of particles $N_\mu(V)$ as function of volume is substituted in the pressure equation. Upon solving this pressure equation (Eq. 28), one obtains the number of adsorbed particles $N_{\mu P}$ and the unit cell volume $V_{\mu P}$ as a function of chemical potential and pressure. At this point, the set of control variables (μ, P) is reduced to a single variable, either being μ or P. As in experiments, the chemical potential and pressure are assumed to be coupled by means of the equation of state $P = P(\mu)$, meaning that the pressure can be interpreted as the vapor pressure outside the MOF. From now on most of our results will be given in terms of the vapor pressure outside the MOF, although an equivalent interpretation could be given in terms of the chemical potential. The resulting adsorption isotherms (not shown) are identical to the ones reported in our previous work[22]. A full discussion of the isotherms may be found there.

4.1.3 Connection with the osmotic potential

Using the computed profile of the number of particles, one can construct the osmotic potential $\tilde{X}_{\mu P}(N_\mu(V), V)$ as a function of volume (see Fig. 6).

This osmotic potential is the important quantity as stable thermodynamic equilibria correspond to minima of this potential. It can be observed that several local minima may exist at different volumes for the same chemical potential. Thermodynamically, only the absolute minimum is the stable solution. However, a phase transition of the material is the result

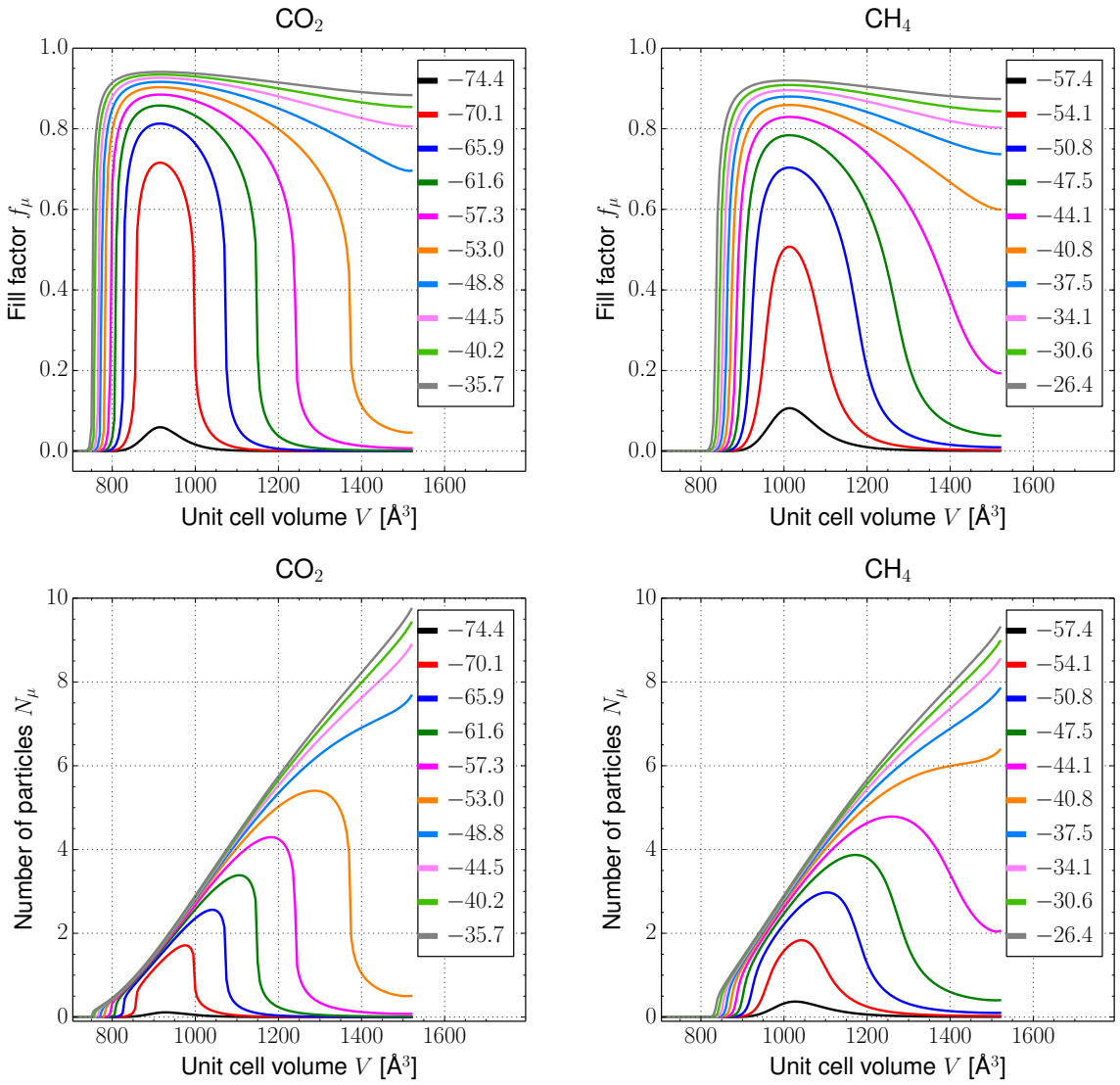

Figure 5. The fill factor f_μ (top) and number of particles N_μ (bottom) as function of unit cell volume for several values of the chemical potential for carbon dioxide (left) and methane (right) in MIL-53(Cr). The chemical potentials μ are indicated in kJ mol $^{-1}$.

of a collective transition. Indeed, one can assume that no individual unit cell transitions of the unit cell volume are allowed and that the entire framework must undergo any unit cell transformation in a collective fashion. This assumption of collective behavior implies that even the slightest barrier in the osmotic potential of a single unit cell translates in a huge barrier for the entire system, which can never be overcome through thermal fluctuations. This means that if the system is in a state represented by a (local) minimum in the osmotic potential, it will stay in that state as long as there is a non-zero barrier separating it from a lower minimum. Therefore, a transition will only occur when a local minimum disappears. More information on the collective phase transitions can be found in Ref. 22 and references therein. Keeping this in mind, one can deduce whether or not adsorbed species will induce breathing in MIL-53(Cr) upon adsorption or not.

Suppose the empty MOF is prepared in the large pore (ca. 1480 Å^3). In the case of methane adsorption, it is observed that the large pore minimum never disappears. There are intermediate values for the chemical potential for which the narrow pore minimum occurs and is even more stable than the large pore minimum, but due to the non-vanishing barrier and local minimum

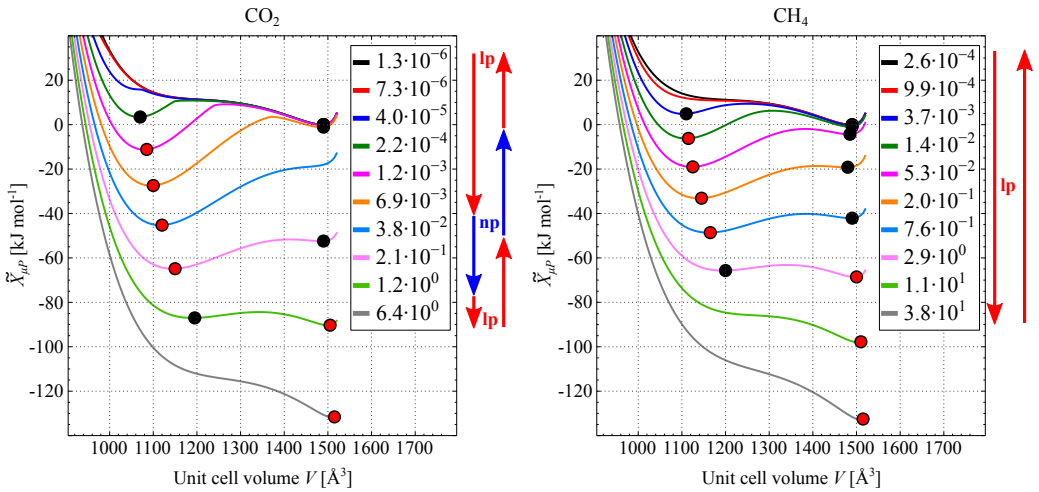

Figure 6. The osmotic potential $\tilde{X}_{\mu P}$ as a function of unit cell volume for several values of the vapor pressure P for carbon dioxide (left) and methane (right) in MIL-53(Cr). The vapor pressures P are indicated in bar. The absolute minimum is indicated with a red dot and a possible second local minimum is represented by a black dot. The arrows to the right of each pane indicate the expected phase during adsorption (arrows pointing down) and desorption (arrows pointing up).

for the large pore, the phase transition will not occur. As such, methane will not induce a breathing transition to the narrow pore upon adsorption. For carbon dioxide on the other hand, the lp minimum vanishes at a pressure of approximately $3.8 \cdot 10^{-2}$ bar. These observations are in agreement with experiments[31].

4.1.4 Connection with adsorption stress

At this point it is interesting to compare our model to earlier proposed theoretical models to explain the conditions for breathing. Neimark et al.[19] introduced the so-called adsorption stress, to rationalize the underlying driving force for breathing. This is the stress (or pressure) the guest molecules inside the pore exert on the host framework. It corresponds to the picture that the pore represents a container with interacting molecules. In this work, the adsorption stress naturally follows from the separation of the free energy profile in the three different parts (Eq. 28) and the mean-field approximation for the interaction. The adsorption stress is in our model due to the guest-guest interaction (Eq. 30) and the guest-host interaction (Eq. 31):

$$P_{\text{ads},\mu}(V) = P_{\text{guest},\mu}(V) + P_{\text{int},\mu}(V) \tag{34}$$

Fig. 7 shows $P_{\text{ads},\mu}$ profiles for several values of the chemical potential. Very small volumes (smaller then 1000 Å^3) typically have a large positive adsorption stress. This means that particles adsorbing in these small unit cells ($2 - -3$ particles as can be seen in Fig. 5) exert a large pressure trying to expand the unit cell. The repulsion between the guest particles, i.e. the P_{guest} contribution, resists the tight confinement in the pores.
The behavior at larger unit cells is more complicated. Two regimes can be identified: at low chemical potential or low vapor pressures the large pore (around 1480 Å^3) has negligible adsorption pressure because no particles will adsorb in the large pore (see lower panes of Fig. 5), while at higher chemical potential (or higher vapor pressure) the large pore has a negative adsorption pressure due to the interaction of the adsorbed particles with the MOF framework, i.e. the P_{int} contribution. It is exactly this negative adsorption pressure that may induce breathing.

Furthermore, following the work of Neimark et al.[19], the condition for a lp to np transition

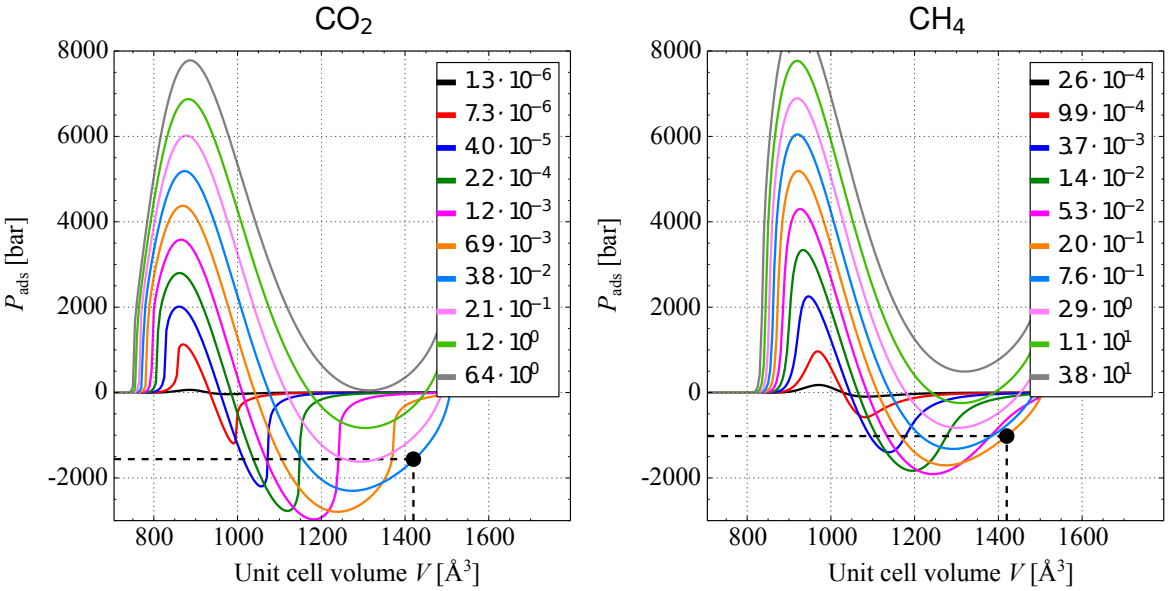

Figure 7. The adsorption pressure $P_{\mathrm{ads},\mu}$ as a function of unit cell volume for several values of the vapor pressure P for carbon dioxide (left) and methane (right) in MIL-53(Cr). The vapor pressures P are indicated in bar.

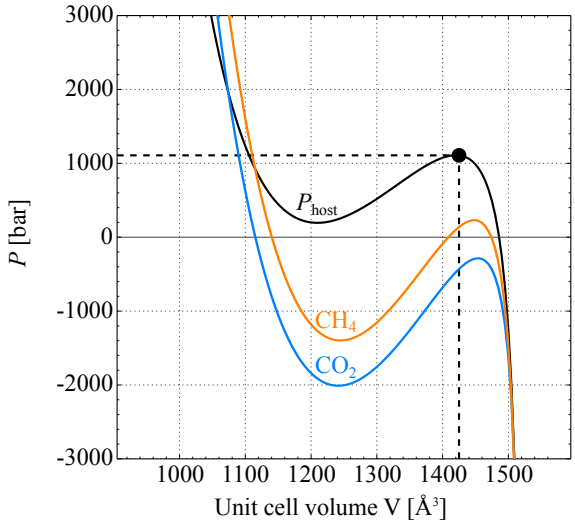

Figure 8. (Black) The pressure profile of the empty host as a function of unit cell volume, taken from the Supporting Information of Ref. 22. (Orange) The total pressure $P_{\mathrm{host}} + P_{\mathrm{ads},\mu}$ profile for methane for a vapor pressure of $2.0 \cdot 10^{-1}$ bar. (Blue) The total pressure $P_{\mathrm{host}} + P_{\mathrm{ads},\mu}$ for carbon dioxide for a vapor pressure of $3.8 \cdot 10^{-2}$ bar.

can be formulated in terms of this adsorption stress. First, the pressure equilibrium equation is rewritten in terms of the adsorption stress:

$$P = P_{\mathrm{host}}(V) + P_{\mathrm{ads},\mu}(V) \tag{35}$$

The left hand side of this equation is the external mechanical pressure exerted on the framework. As was mentioned before, this mechanical pressure is related to the chemical potential by means of the equation of state of the adsorbent species in the environment. In all common experimental setups, this pressure will only amount to an order of magnitude of 1 bar. The pressure of the empty host profile is shown in Fig. 8. The typical order of magnitude for this pressure amounts to about 1000 bar for unit cells with a volume of 1420 $\mathrm{\AA}^3$ and thus on this scale the external mechanical pressure is negligible. To deduce a quantitative criterion for a phase transition, one

could approximate this external pressure to be zero. This assumption was also applied by Coudert et al. who omitted the PV term in the osmotic potential[17]. At this point one can solve Eq. (35) and determine the appropriate volume for several values of the chemical potential (and resulting vapor pressure). The solution is found at the intersect of the $P_{\text{host}}(V) + P_{\text{ads},\mu}(V)$ curve with the horizontal $P = 0$ line.
Following observations can be made :

- At low chemical potential, the pores of the framework are empty since the driving force for adsorption is too low and the adsorption stress will be zero, which means we need to look for the solution of $P_{\text{host}}(V) = 0$. From Fig. 8 one can see that this means that Eq. (35) will only have one solution at $V \approx 1480$ Å^3, which is also stable (because it has a negative slope) and thus the system will reside in the large pore phase.
- When the chemical potential increases, the adsorption stress will become non-zero and obtain a negative value at high volumes. As a result the curve of $P_{\text{host}}(V) + P_{\text{ads},\mu}(V)$ will shift to lower pressures at high volumes ($1100 - 1500$ Å^3). This is illustrated for CO_2 for a pressure of $2.0 \cdot 10^{-1}$ bar (blue curve on Fig. 8) and for CH_4 at a pressure of $3.8 \cdot 10^{-2}$ bar (orange curve in Fig. 8). As was mentioned before in Section 4.1.3, for a breathing transition to occur in a concerted fashion, a local minimum of the osmotic ensemble $\tilde{X}_{\mu P}$ must disappear. This condition can be translated in terms of the pressure $P_{\text{host}}(V)+P_{\text{ads},\mu}(V)$: an intersect with the horizontal $P = 0$ (with negative slope) must disappear. Hence, when the maximum of P_{host} located at 1420 Å^3 shifts down below zero under the influence of the adsorption stress $P_{\text{ads},\mu}$, no intersect with $P = 0$ will exist anymore at the large pore, and the system will be forced to transform to the narrow pore (where there is an intersect). Indeed for CO_2 the blue curve shifts completely below zero, while for CH_4 this is not the case. This is in agreement with the experimental observation that MIL-53(Cr) breathes under influence of CO_2 but not for CH_4.

Finally, the condition for a lp to np transition under influence of adsorption can be formulated as follows. The framework exhibits a lp to np transition if there exists a value for the chemical potential for which the adsorption stress at 1420 Å^3 is lower than -1100 bar. The most negative value of the adsorption stress at 1420 Å^3 for methane is approximately -1000 bar (at a vapor pressure of $2.0 \cdot 10^{-1}$ bar) and for carbon dioxide it is approximately -1700 bar (at a vapor pressure of $3.8 \cdot 10^{-2}$ bar). Previous rationalization shows that our model confirms the qualitative model predicted by Coudert et al. to predict the conditions for breathing.

4.2 *Case study II: adsorption of xenon in MIL-53(Al)*

4.2.1 Free energy profile of MIL-53(Al)

Using the methodology outlined in Section 2.1.1, the free energy F_{host} is computed of the empty MIL-53(Al) framework (Fig. 9). An average error is estimated at 0.16 kJ mol^{-1} by running two distinct molecular dynamics simulations with slightly different initial conditions. This profile illustrates the bistability of this MOF: two stable structures exist, characterized by minima in the free energy profile. The volume of the large pore structure is seen to be $V_{\text{lp}} = 1450$ Å^3, while the narrow pore corresponds to a volume of $V_{\text{np}} = 820$ Å^3, which corresponds to a relative contraction of 43% (see also Fig. 1). These values compare well with experimental values of 1424–1428 Å^3 (lp) and 860–900 Å^3 (np)[6, 9]. Moreover, it is seen that the np minimum is more stable than the lp minimum, corresponding to a difference in free energy of 26.5 kJ mol^{-1}. Keeping in mind the collective behavior (see Section 4.1.3), which implies not even the smallest barrier can be overcome, the lp structure will not collapse to the np structure without any external stimuli due to the presence of a small barrier of $\sim$2 kJ/mol at 300 K. This is in agreement with the experiments done by Liu et al.[6]: a temperature of 300 K is still in the region of hysteresis, where both lp and np structures can be observed depending on their history. However, due to an overestimation of the dispersion interactions, it may be that the free energy difference between

np and lp is overestimated as well. Indeed, already at 0 K, the energy difference between np and lp is very sensitive to the magnitude of the van der Waals interactions[13].

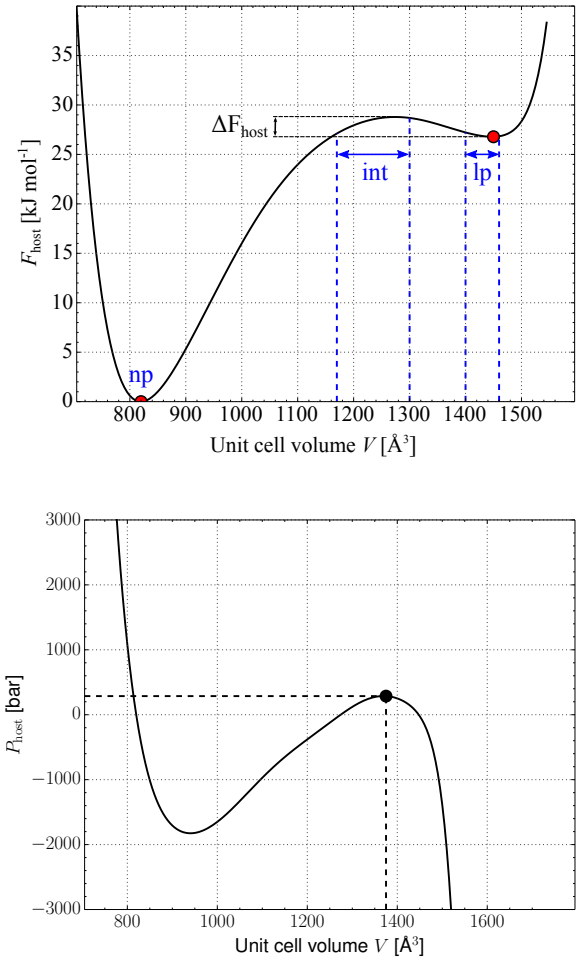

Figure 9. (Top) The host free energy as a function of unit cell volume for MIL-53(Al) at 300 K. The average error on the free energy is 0.16 kJ mol ^{1}. (Bottom) The corresponding pressure profile of the emtpy host as function of unit cell volume for MIL-53(Al).

The pressure of the empty host P_{host} (Eq. 17) is plotted in the bottom pane of Fig. 9 and can be used to deduce transition pressures. Assume a sample is prepared in lp. The maximal pressure for which the material remains in the lp structure hence corresponds to the local maximum in the pressure profile close to the large pore. From Fig. 9 we can deduce that this transition pressure is expected to be 310 bar, in good agreement with the experimental transition pressure of 130 to 180 bar[9]. Likewise, a transition pressure for the expansion of the np to lp structure corresponds to the minimum in the vicinity of the np structure. Based on our simulation, this transition pressure amounts to 1830 bar, an order of magnitude larger than the lp to np transition pressure. This negative np-lp transition pressure is not observed experimentally[9], because the experimental setup is not able to apply negative pressure. The fact that the np-lp transition is experimentally not observed at a positive pressure, and hence has to be at a negative pressure, confirms that the np is still represented by a local minimum in the free energy profile.

4.2.2 Xenon adsorption in MIL-53(Al)

In this section our model is applied to study the adsorption of xenon in MIL-53(Al). The results of the Monte Carlo calculations of the pore volume and the interaction energy can be

found in Section 7 of the Supporting Information. The workflow to study phase transitions under the stimulus of adsorbed guest molecules is similar as for MIL-53(Cr). The chemical potential and pressure equation are solved under the assumption that the external pressure is exerted by the gas only, as in an experimental setup. P and μ are thus coupled by the van der Waals equation of state of xenon.

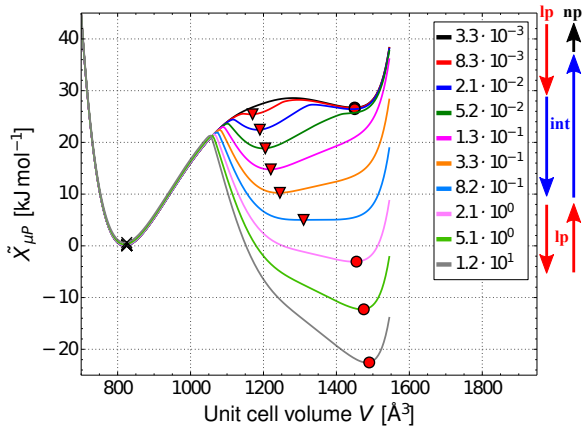

Figure 10. Osmotic potential $\tilde{X}_{\mu P}$ of MIL-53(Al) with xenon as a function of unit cell volume V for several values of the vapor pressure P. The vapor pressures P are indicated on the figure in bar. A circle represents the lp phase, a triangle represents the int phase and a cross represents the np phase. The arrows on the right indicate the expected phase during adsorption (arrows pointing down) and desorption (arrows pointing up).

The osmotic potential $\tilde{X}_{\mu P}$ as a function of unit cell volume is shown in Fig. 10. Three types of (meta)stable equilibria emerge :

(1) The first is the empty np phase (indicated by a cross on Fig. 10) with a volume of $V_{\text{np}} = 820$ Å^3. At every value of the chemical potential/vapor pressure, the empty np phase remains a (meta)stable equilibrium. This np phase corresponds to the narrow pore as observed by Liu et al.[6] of the empty host and identified by our force field calculations in an earlier work[13].

(2) The second type of equilibrium is a large pore structure (indicated by a circle on Fig. 10) with a volume similar to the empty lp phase ($V_{\text{lp}} = 1400 - 1460$ Å^3), but which does include adsorbed particles.

(3) The third type of equilibrium is an intermediate structure (indicated by a triangle on Fig. 10), with a volume within a wide range ($V_{\text{int}} = 1170 - 1300$ Å^3) and which also includes adsorbed particles. We will compare our results with the experimental and theoretical study of Boutin et al.[15], in which this phase is denoted as np. However we will denote this phase as int, to make the distinction with the empty np phase and to be consistent with the work of Bousquet et al.[16][15]. Boutin et al.[15] used the thermodynamic model of Coudert et al.[17] to determine the relative stability of two phases with a well defined volume: a large pore with a volume $V_{\text{lp}} = 1419$ Å^3 and a intermediate pore with a volume that is 23.5 % smaller than the lp volume ($V_{\text{int}} = 1085$ Å^3).

We will now discuss the relative stability of these phases. If the sample was initially prepared in np, our model predicts that it will stay in np, whatever the applied pressure, and hence it will not adsorb any xenon. This is due to xenon being simply to big to fit in the np structure. In other words, a sample prepared in the np phase appears to be non-porous for xe-adsorption. To the best of our knowledge, this behavior has not been tested experimentally. In most experimental setups so far, the sample is prepared in the lp phase as the material will be outgassed at high temperature. In that case, our model does predict adsorption of xenon and

breathing. Indeed starting at low vapor pressure yields the large pore phase. From a pressure of $5.2 \cdot 10^{-2}$ bar (or the dark green curve in Fig. 10), the lp minimum disappears and a new phase is predicted to occur, the intermediate phase (int)[15]. Care must be taken that this phase has a larger volume than the empty np and contains adsorbed xenon and is thus different from the np phase of the empty host. Further increasing the pressure maintains the int phase up to pressures lower then $8.2 \cdot 10^{-1}$ bar where the int phase minimum disappears and the system goes back to the lp phase, containing adsorbed xenon atoms. Our model further predicts that a desorption experiment starting from this lp phase, would induce a transition to the int phase at $0.82 - 2.06$ bar and would transform to the empty np when lowering the pressure even further. The system would not return to the lp phase as a small but non-negligible barrier remains between int and lp.

An intermediate result of Boutin et al. is an estimation of the difference in free energy between these two phases based on experimental isotherms[15][1]: $\Delta F_{\text{host}} = F_{\text{lp}} - F_{\text{int}} \approx -8\ \text{kJ mol}^{-1}$. Furthermore, Devautour-Vinot et al[32]. estimated a value of $\Delta H_{\text{host}} \approx 20\ \text{kJ mol}^{-1}$, also based on experiments, which results in $\Delta F_{\text{host}} \approx -2.2\ \text{kJ mol}^{-1}$. In our model, the difference in free energy can be determined from Fig. 9. Taking into account the range of volumes for both the lp and int phases, we arrive at a free-energy difference between -2.0 and $0.1\ \text{kJ mol}^{-1}$, which is in good agreement with the previously reported numbers.

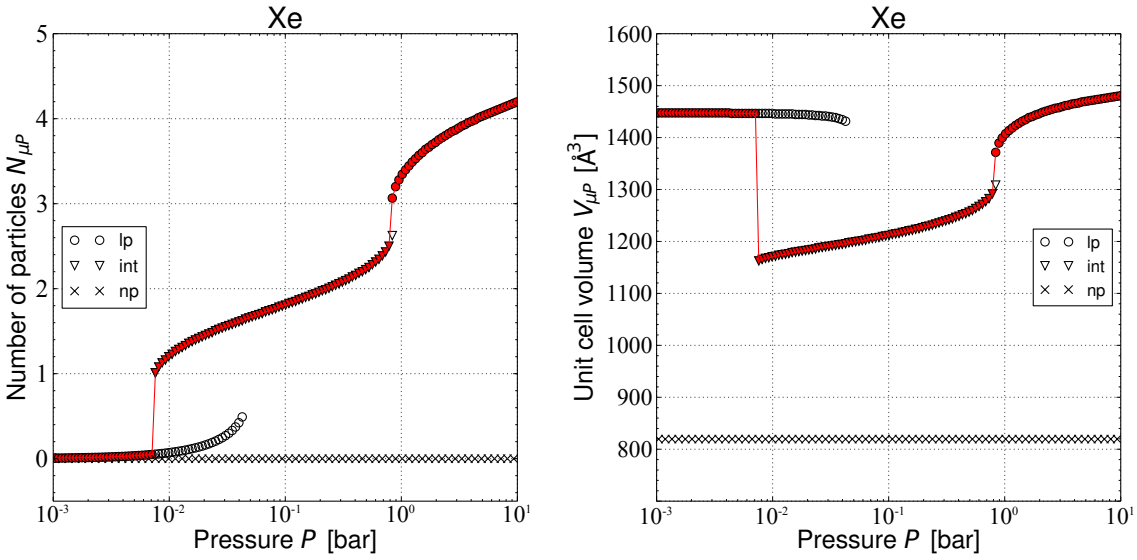

Figure 11. Number of adsorbed particles (left) and unit cell volume (right) as a function of vapor pressure for xenon adsorption in MIL-53(Al). The circles and triangles represent the equilibrium phases in which particles can adsorb, i.e. the lp and int phases respectively. When a circle/triangle is filled red, the lp/int is the most stable adsorbed state. When the circle and triangle are not filled, both adsorption states are (meta)stable at that pressure. The black crosses represent the empty state np, which cannot accommodate any guest molecules, but is a (meta)stable equilibrium at every vapor pressure.

The adsorption isotherm $N_{\mu P}$ and the unit cell volume $V_{\mu P}$ is plotted in Fig. 11 as a function of pressure P. One can clearly identify two transitions on the adsorption isotherm. The phase transitions throughout the adsorption/desorption process can be summarized in the following

[1]Strictly speaking, Boutin et al. determined ΔG. However, at the low pressures involved in adsorption experiments the difference between free enthalpy and free energy is neglegible.

scheme:

$$\begin{array}{lrcccl} \underline{\text{adsorption}}: & \text{lp } (1450\ \mathring{\text{A}}^3) & \rightarrow & \text{int } (1170-1300\ \mathring{\text{A}}^3) & \rightarrow & \text{lp } (1400-1460\ \mathring{\text{A}}^3) \\ \underline{\text{desorption}}: & \text{np } (820\ \mathring{\text{A}}^3) & \leftarrow & \text{int } (1170-1300\ \mathring{\text{A}}^3) & \leftarrow & \text{lp } (1400-1460\ \mathring{\text{A}}^3) \end{array}$$

All transitions represent first-order transitions with hysteresis. The first transition occurs at $0.006 - 0.04$ bar, while the second transition occurs at $2.0 - 2.5$ bar. As such, the model is able to confirm that xenon adsorption induces breathing behaviour in MIL-53(Al), as is also observed experimentally[15]. In those experiments, the first transition occurs at $0.2 - 0.5$ bar for 292 K, while the second transition was not observed within a range of $0 - 1.5$ bar. Similarly as for carbon dioxide adsorption in MIL-53(Cr) in Ref. 22, our model predicts transition pressures that are too low. The number of particles that adsorb in the int phase is around two particles, in good agreement with the experiments of Boutin et al. A last observation concerns the end state of the desorption branch. In the scheme above, the final state of the desorption branch is identified as the np phase, i.e. the narrow pore equilibrium of the empty framework. The underlying reason is clearly visible on a plot of the osmotic potential (see Fig. 10). When the chemical potential is decreased, starting from the filled lp at large vapor pressure, one can see the material transforming back to the filled int state. Decreasing the chemical potential even further, one can see that the barrier in the osmotic potential that separates the int from the lp never vanishes. On the other hand, the barrier separating the int from the np phase does vanish. Hence, the model predicts that every desorption experiment will leave the material in the empty np phase. This observation cannot be verified by means of the result of Boutin et al., because the accuracy on the measured number of particles is too low to distinguish between int and np. Furthermore, no information on the unit cell volume of the several phases is available. This peculiar behavior is a prediction of the model that, to the best of our knowledge, has not yet been observed experimentally. It can, however, be linked with the thermodynamic investigation of Bousquet et al.[16] They introduced the so-called most comfortable state (MCS) which represents the state of the MOF in which the guest molecules have the most attractive interactions and are hence in their most comfortable state. In the case of xenon in MIL-53(Al), the MCS is located between the np minimum and the local maximum in the free energy profile, but closest to the maximum. As such the np and int states are well separated with a non-zero barrier in between and once the MOF reaches np, it will stay there due to this barrier.

5 Conclusions

In this paper we proposed a semi-analytical model to unravel and predict the breathing behavior of flexible materials. All input parameters can be determined from molecular dynamics simulations. However to compare with experimental adsorption–desorption isotherms, it is essential to describe the thermodynamics of the system in an osmotic ensemble in terms of the chemical potential of the adsorbant species, the mechanical pressure and the temperature. The original free energy is transformed to the osmotic ensemble using a Legendre transform. In this work a semi-analytical solution is proposed to determine the equilibrium conditions for the chemical potential and pressure. A new quantity is introduced, the fill factor, which represents the degree to which the pores are filled. Our equilibrium conditions and osmotic potential can be expressed in terms of this easy to interpret fill factor.

The new model is tested on adsorption of CO_2 and CH_4 in MIL-53(Cr) and adsorption of xenon in MIL-53(Al). The first case study is used as a proof of concept study as it has been examined by various authors in the past. Our model confirms the results found earlier in literature: MIL-53(Cr) shows a breathing behavior upon adsorption of CO_2 whereas it remains in its large pore shape during an adsorption-desorption experiment with CH_4. Conditions for

breathing were earlier proposed by Coudert et al. and rationalized in terms of an adsorption pressure. This last quantity directly follows from our model and indeed confirms the hypothesis put forward by Neimark et al.[19]

For MIL-53(A), a slightly different behavior is found. First, all input parameters required for our semi-analytic thermodynamic model are determined using no empirical input but solely from molecular simulations. The host free energy profile was determined from molecular dynamics simulations where the volume was fixed but for which the shape could still vary. The interaction of the particles with the host matrix was determined from Monte Carlo simulations. The osmotic potential indeed confirms the experimentally observed behavior. When starting from a lp phase the structure switches to a intermediate phase form for a higher vapour pressure of the gas molecules. Upon increasing the vapour pressure even more, the system switches back to the lp form. In a consecutive desorption experiment, the system first reverts to the intermediate phase after decreasing the vapour pressure and finally switches to an empty narrow pore instead of an empty large pore. When one would start an adsorption-desorption cycle from the np form, our model predicts that the material would not breathe, indicating that breathing depends on the history of the system.

The proposed theoretical model gives complementary insights into the breathing behavior and has the potential to be applied to other flexible materials. The user needs to be able to determine the separate contributions to the free energy of the system.

Acknowledgement

This work is supported by the Fund for Scientific Research; Flanders (FWO), the Research Board of Ghent University (BOF) and BELSPO in the frame of IAP/6/27. Funding was also received from the European Research Council under the European Community's Seventh Framework Programme [FP7(2007-2013) ERC grant agreement number 240483]. Computational resources (Stevin Supercomputer Infrastructure) and services were provided by Ghent University.

References

[1] S. Kitagawa, R. Kitaura, and S.i. Noro, *Functional Porous Coordination Polymers*, Angewandte Chemie International Edition 43 (2004), pp. 2334–2375.

[2] A.R. Millward and O.M. Yaghi, *MetalOrganic Frameworks with Exceptionally High Capacity for Storage of Carbon Dioxide at Room Temperature*, Journal of the American Chemical Society 127 (2005), pp. 17998–17999.

[3] G. Ferey and C. Serre, *Large breathing effects in three-dimensional porous hybrid matter: facts, analyses, rules and consequences*, Chem. Soc. Rev. 38 (2009), pp. 1380–1399.

[4] A. Schneemann, V. Bon, I. Schwedler, I. Senkovska, S. Kaskel, and R. Fischer, *Flexible metal-organic frameworks*, Chem. Soc. Rev. 43 (2014), pp. 6062–6096.

[5] C. Serre, F. Millange, C. Thouvenot, M. Noguès, G. Marsolier, D.A. Louër, and G. Férey, *Very Large Breathing Effect in the First Nanoporous Chromium(III)-based Solids: MIL-53 or Cr(III)(OH) x [O(2)C-C(6)H(4)-CO(2)] x [HO(2)C-C(6)H(4)-CO(2)H](x) x H(2)O(y)*, J. Am. Chem. Soc. 124 (2002), pp. 13519–13526.

[6] Y. Liu, J. Her, A. Dailly, A. Ramirez-Cuesta, D. Neumann, and C. Brown, *Reversible Structural Transition in MIL-53 with Large Temperature Hysteresis*, J. Am. Chem. Soc. 130 (2008), pp. 11813–11818.

[7] A. Ghoufi, A. Subercaze, Q. Ma, P.G. Yot, Y. Ke, I. Puente-Orench, T. Devic, V. Guillerm, C. Zhong, C. Serre, G. Férey, and G. Maurin, *Comparative Guest, Thermal, and Mechanical Breathing of the Porous Metal Organic Framework MIL-53(Cr): A Computational Exploration Supported by Experiments*, 116 (2012), pp. 13289–13295.

[8] A. Boutin, D. Bousquet, A.U. Ortiz, F.X. Coudert, A.H. Fuchs, A. Ballandras, G. Weber, I. Bezverkhyy, J.P. Bellat, G. Ortiz, G. Chaplais, J.L. Paillaud, C. Marichal, H. Nouali, and J. Patarin, *Temperature-Induced Structural Transitions in the Gallium-Based MIL-53 Metal–Organic Framework*, 117 (2013), pp. 8180–8188.

[9] P. Yot, Z. Boudene, J. Macia, D. Granier, L. Vanduyfhuys, T. Verstraelen, V.V. Speybroeck, T. Devic, C. Serre, G. Férey, N. Stock, and G. Maurin, *Metal-organic frameworks as potential shock absorbers: the case of the highly flexible MIL-53(Al).*, Chem Commun (Camb) 50 (2014), pp. 9462–9464.

[10] T. Loiseau, C. Serre, C. Huguenard, G. Fink, F. Taulelle, M. Henry, T. Bataille, and G. Ferey, *A Rationale for the Large Breathing of the Porous Aluminum Terephthalate (MIL-53) Upon Hydration*, Chem.Eur.J. 10 (2004), pp. 1373–1382.

[11] C. Volkringer, T. Loiseau, N. Guillou, G. Ferey, E. Elkaim, and A. Vimont, *XRD and IR structural investigations of a particular breathing effect in the MOF-type gallium terephthalate MIL-53(Ga)*, Dalt. Trans. (2009), pp. 2241–2249.

[12] A. Walker, B. Civalleri, B. Slater, C. Mellot-Draznieks, F. Corà, C.M. Zicovich-Wilson, G. Román-Pérez, J.M. Soler,

and J. Gale, *Flexibility in a Metal–Organic Framework Material Controlled by Weak Dispersion Forces: The Bistability of MIL-53(Al)*, Angew. Chem. Int. Ed. 49 (2010), pp. 1–4.

[13] L. Vanduyfhuys, T. Verstraelen, M. Vandichel, M. Waroquier, and V. Van Speybroeck, *Ab Initio Parametrized Force Field for the Flexible MetalOrganic Framework MIL-53(Al)*, J. Chem. Theory Comput. 8 (2012), pp. 3217–3231.

[14] D. Coombes, F. Cora, C. Mellot-Draznieks, and R.G. Bell, *Sorption-Induced Breathing in the Flexible Metal Organic Framework CrMIL-53: Force-Field Simulations and Electronic Structure Analysis.*, J. Phys. Chem. C 113 (2009), pp. 544–552.

[15] A. Boutin, M. Springuel-Huet, A. Nossov, A. Gédéon, T. Loiseau, C. Volkringer, G. Férey, F. Coudert, and A. Fuchs, *Breathing Transistions in Mil-53(Al) Metal-organic framework upon Xenon adsorption.*, Angew; Chem. Int. Ed. 48 (2009), pp. 8314–8317.

[16] D. Bousquet, F.X. Coudert, A. Fossati, A. Neimark, A. Fuchs, and A. Boutin, *Adsorption induced transitions in soft porous crystals: An osmotic potential approach to multistability and intermediate structures*, The Journal of Chemical Physics 138 (2013), p. 174706.

[17] F. Coudert, M. Jeffroy, A.H. Fuchs, A. Boutin, and C. Mellot-Draznieks, *Thermodynamics of Guest-Induced Structural Transitions in Hybrid Organic-Inorganic Frameworks*, J. Am. Chem. Soc. 130 (2008), pp. 14294–14302.

[18] F. Coudert, A. Boutin, and A. Fuchs, *A thermodynamic description of the adsorption-induced structural transitions in flexible MIL-53 metal-organic framework*, Mol. Phys. 112 (2014), pp. 1257–1261.

[19] A.V. Neimark, F. Coudert, A. Boutin, and A.H. Fuchs, *Stress-Based Model for the Breathing of Metal-Organic Frameworks*, J. Phys. Chem. Lett. 1 (2010), pp. 445–449.

[20] C. Triguero, F.X. Coudert, A. Boutin, A.H. Fuchs, and A.V. Neimark, *Mechanism of Breathing Transitions in Metal-Organic Frameworks*, J. Phys. Chem. Lett. 2 (2011), pp. 2033–2037.

[21] D. Bousquet, F.X. Coudert, and A. Boutin, *Free Energy Landscape for the Thermodynamic Understanding of Adsorption-Induced Deformations and Structural Transitions in Porous Materials*, J. Chem. Phys. 137 (2012), p. 044118.

[22] A. Ghysels, L. Vanduyfhuys, M. Vandichel, M. Waroquier, V. Van Speybroeck, and B. Smit, *On the Thermodynamics of Framework Breathing: A Free Energy Model for Gas Adsorption in MIL-53*, J. of Phys. Chem. C 117 (2013), pp. 11540–11554.

[23] G.J. Martyna, D.J. Tobias, and M.L. Klein, *Constant pressure molecular dynamics algorithms*, J. Chem. Phys. 101 (1994), pp. 4177–4189.

[24] N. Allinger, J. Lii, and Y. Yuh, J. Am. Chem. Soc. 111 (1989), pp. 8551–8566.

[25] L. Vanduyfhuys, S. Vandenbrande, T. Verstraelen, R. Schmid, M. Waroquier, and V. Van Speybroeck, *QuickFF: A program for a quick and easy derivation of force fields for Metal-Organic Frameworkds from ab initio input.*, J. Comput. Chem. 36 (2014), pp. 1015–1027.

[26] S. Bureekaew, S. Amirjalayer, M. Tafipolsky, C. Spickermann, T.K. Roy, and R. Schmid, *MOF-FF - A flexible first-principles derived force field for metal-organic frameworks*, 250 (2013), pp. 1128–1141.

[27] J.K. Bristow, D. Tiana, and A. Walsh, *Transferable Force Field for Metal–Organic Frameworks from First-Principles: BTW-FF*, 10 (2014), pp. 4644–4652.

[28] M.A. Addicoat, N. Vankova, I.F. Akter, and T. Heine, *Extension of the Universal Force Field to Metal–Organic Frameworks*, 10 (2014), pp. 880–891.

[29] T. Verstraelen, L. Vanduyfhuys, S. Vandenbrande, S.M.J. Rogge, *Yaff, yet another force field*, http://molmod.ugent.be/software/.

[30] G.J. Martyna, M.L. Klein, and M.E. Tuckerman, *Nos-Hoover chains: The canonical ensemble via continuous dynamics*, J. Chem. Phys. 97 (1992), pp. 2635–2643.

[31] P. Llewellyn, G. Maurin, T. Devic, S. Loera-Serna, N. Rosenbach, C. Serre, S. Bourrelly, P. Horcajada, Y. Filinchuk, and G. Férey, *Prediction of the Conditions for Breathing of Metal Organic Framework Materials Using a Combination of X-ray Powder Diffraction, Microcalorimetry, and Molecular Simulation.*, J. Am. Chem. Soc. 130 (2008), pp. 12808–12814.

[32] A. Devautour-Vinot, G. Maurin, F. Henn, C. Serre, T. Devic, and G. Férey, *Estimation of the breathing energy of flexible MOFs by combining TGA and DSC techniques*, Chem. Commun. (2009), pp. 2733–2735.